Natural Variation within a Species for Traits Underpinning C_4 Photosynthesis[1][CC-BY]

Gregory Reeves,[a,2] Pallavi Singh,[a,2] Timo A. Rossberg,[a] E.O. Deedi Sogbohossou,[b] M. Eric Schranz,[b] and Julian M. Hibberd[a,3]

[a]Department of Plant Sciences, University of Cambridge, Cambridge CB2 3EA, United Kingdom
[b]Biosystematics Group, Department of Plant Sciences, Wageningen University, Wageningen 6700 AA, The Netherlands

ORCID IDs: 0000-0001-9805-4899 (T.A.R.); 0000-0002-9034-0062 (E.O.D.S.); 0000-0001-6777-6565 (M.E.S.); 0000-0003-0662-7958 (J.M.H.).

Engineering C_4 photosynthesis into C_3 crops could substantially increase their yield by alleviating photorespiratory losses. This objective is challenging because the C_4 pathway involves complex modifications to the biochemistry, cell biology, and anatomy of leaves. Forward genetics has provided limited insight into the mechanistic basis of these properties, and there have been no reports of significant quantitative intraspecific variation of C_4 attributes that would allow trait mapping. Here, we show that accessions of the C_4 species *Gynandropsis gynandra* collected from locations across Africa and Asia exhibit natural variation in key characteristics of C_4 photosynthesis. Variable traits include bundle sheath size and vein density, gas-exchange parameters, and carbon isotope discrimination associated with the C_4 state. The abundance of transcripts encoding core enzymes of the C_4 cycle also showed significant variation. Traits relating to water use showed more quantitative variation than those associated with carbon assimilation. We propose that variation in these traits likely adapted the hydraulic system for increased water use efficiency rather than improving carbon fixation, indicating that selection pressure may drive C_4 diversity in *G. gynandra* by modifying water use rather than photosynthesis. The accessions analyzed can be easily crossed and produce fertile offspring. Our findings, therefore, indicate that natural variation within this C_4 species is sufficiently large to allow genetic mapping of key C_4 traits and regulators.

Plants that use C_4 photosynthesis can effectively abolish photorespiratory losses that occur when Rubisco fixes oxygen rather than CO_2 (Bowes et al., 1971; Sharkey, 1988). In C_4 plants, Rubisco is typically sequestered in bundle sheath (BS) cells that are concentrically arranged around the vasculature. The establishment of a molecular CO_2 pump delivers carbon to Rubisco from mesophyll (M) cells via C_4 acid intermediates (Garner et al., 2001). C_4 photosynthesis relies more heavily on the BS for photosynthesis and less on M cells. It also involves more chloroplasts in BS cells, an increased proliferation of plasmodesmata between M and BS cells, and a higher vein density to increase the volume of the leaf occupied by the BS. These morphological alterations to the leaf that facilitate the C_4 cycle are known as Kranz anatomy (Langdale, 2011; Lundgren et al., 2014). Moreover, photosynthesis gene expression is modified such that genes encoding components of the C_4 and Calvin-Benson-Bassham cycles are strongly and preferentially expressed in either M or BS cells (Garner et al., 2001; Marshall et al., 2007; Hibberd and Covshoff, 2010).

Despite the complex modifications associated with C_4 photosynthesis, current estimates are that the C_4 pathway has independently evolved more than 60 times in angiosperms (Sage, 2016), which suggests that a relatively straightforward route may allow the transition from the ancestral C_3 state to the derived C_4 state. A number of factors appear to have facilitated this apparently complex transition. First, proteins of the C_4 pathway operate in the ancestral C_3 state (Hibberd and Quick, 2002; Brown et al., 2010; Eastmond et al., 2015). Second, the modifications to gene expression associated with C_4 leaves appear to have been built on partly preexisting regulatory architecture found in C_3 species (Brown et al., 2011; Kajala et al., 2012; Burgess et al., 2016; Williams et al., 2016; Reyna-Llorens et al., 2018). Moreover, after a binary categorization of phenotypes into either C_3 or C_4, mathematical modeling indicates that there is likely more than one route from which to acquire the C_4 state (Williams et al., 2013) but that subsequent modifications, many of which are associated with rebalancing photorespiration, reinforce these improvements in photosynthesis and fitness (Heckmann et al., 2013; Mallmann et al., 2014; Bräutigam and Gowik, 2016).

Genome-wide analysis of transcript abundance in multiple C_3 and C_4 species has provided unbiased in-

[1]G.R. was supported by a Gates Cambridge Trust PhD Fellowship and P.S. by Advanced European Research Council grant 694733 Revolution to J.M.H.

[2]These authors contributed equally to the article.

[3]Address correspondence to jmh65@cam.ac.uk.

The author responsible for distribution of materials integral to the findings presented in this article in accordance with the policy described in the Instructions for Authors (www.plantphysiol.org) is: Julian M. Hibberd (jmh65@cam.ac.uk).

G.R., P.S., and J.M.H. designed the study; G.R., P.S., T.A.R., and E.O.D.S. carried out experimental work; G.R., P.S., T.A.R., M.E.S., and J.M.H. wrote the article.

www.plantphysiol.org/cgi/doi/10.1104/pp.18.00168

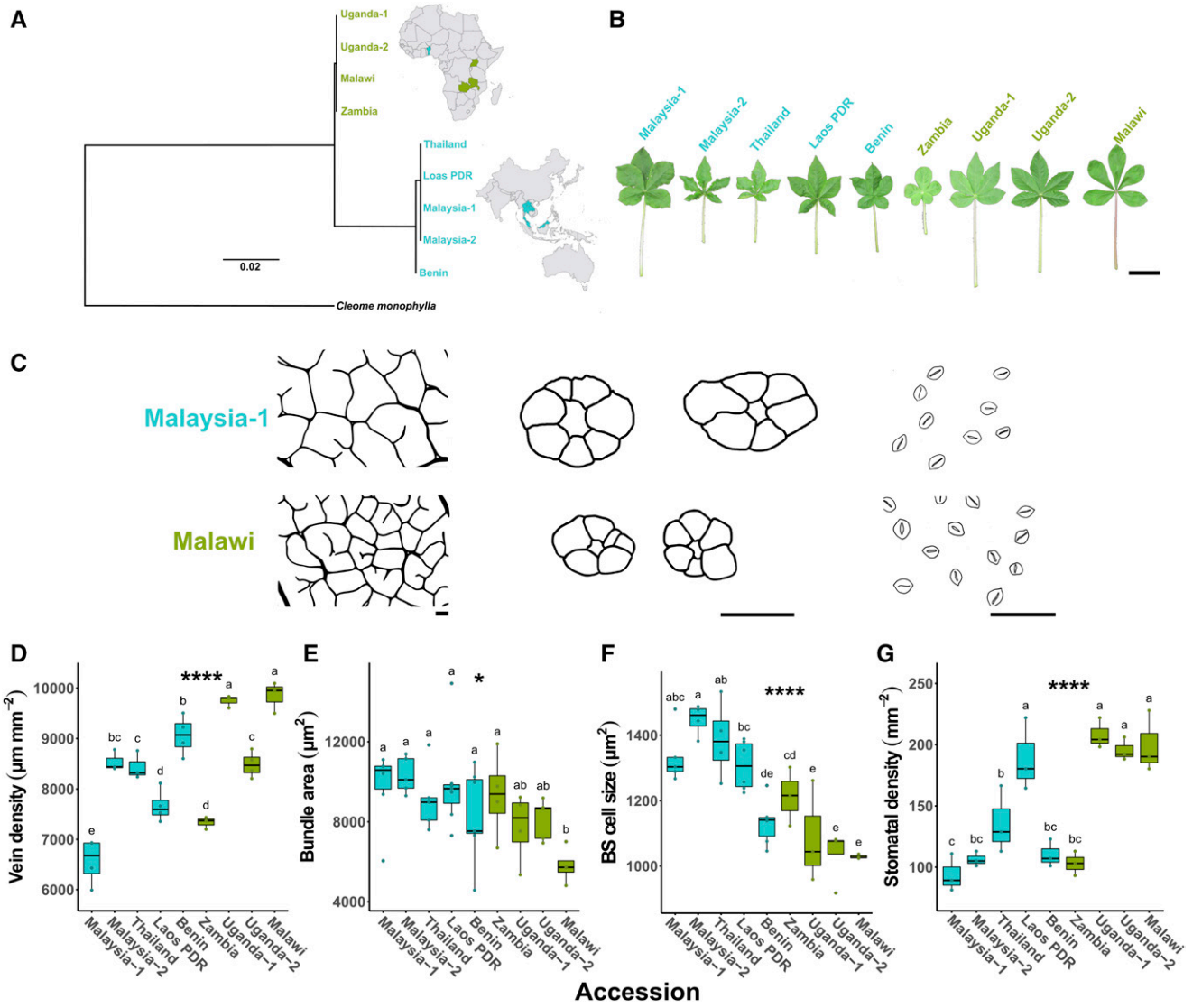

Figure 1. Natural variation in Kranz anatomy among a diverse panel of *G. gynandra* accessions. A, Geographic and phylogenetic relationships for nine accessions from seven countries across Africa and Asia. B, Variation in fully mature whole leaves of 6-week-old plants. C, Traces indicate variation in venation, bundle area, BS cell size, and stomatal density of fully mature leaves for two extreme accessions. D to G, Vein density (D), bundle area (E), BS cell size (F), and stomatal density (G) for all accessions. Asterisks indicate significant differences between accessions (one-way ANOVA: *, $P < 0.05$; and ****, $P < 0.0001$). Letters above individual box-scatterplots indicate significant groupings according to Duncan's multiple range test ($\alpha = 0.05$). The number of replicates for each accession ranged from three to seven. Bars = 5 cm (B) and 100 µm (C).

sight into processes that likely change in C_4 compared with C_3 leaves (Aubry et al., 2014; Bräutigam et al., 2014; Lauterbach et al., 2017). Furthermore, cis-elements that control the expression of genes encoding components of the C_4 cycle have been documented (Akyildiz et al., 2007; Williams et al., 2016; Reyna-Llorens et al., 2018). However, the regulators that recognize these motifs have not been isolated (Reeves et al., 2017). Thus, despite the progress in our understanding of C_4 photosynthesis, it is currently not possible to rationally design a C_4 pathway in a C_3 leaf.

When natural variation is present, the development of a mapping population enables molecular marker-trait associations by methods such as quantitative trait locus mapping and genome-wide association studies. Molecular marker-trait association studies help delineate genomic regions associated with trait variation. Fine genetic mapping of these genomic regions with major effects allows the identification of causal genes underpinning the variation. Such approaches have been used extensively to map loci responsible for numerous complex traits in plants (Mauricio, 2001).

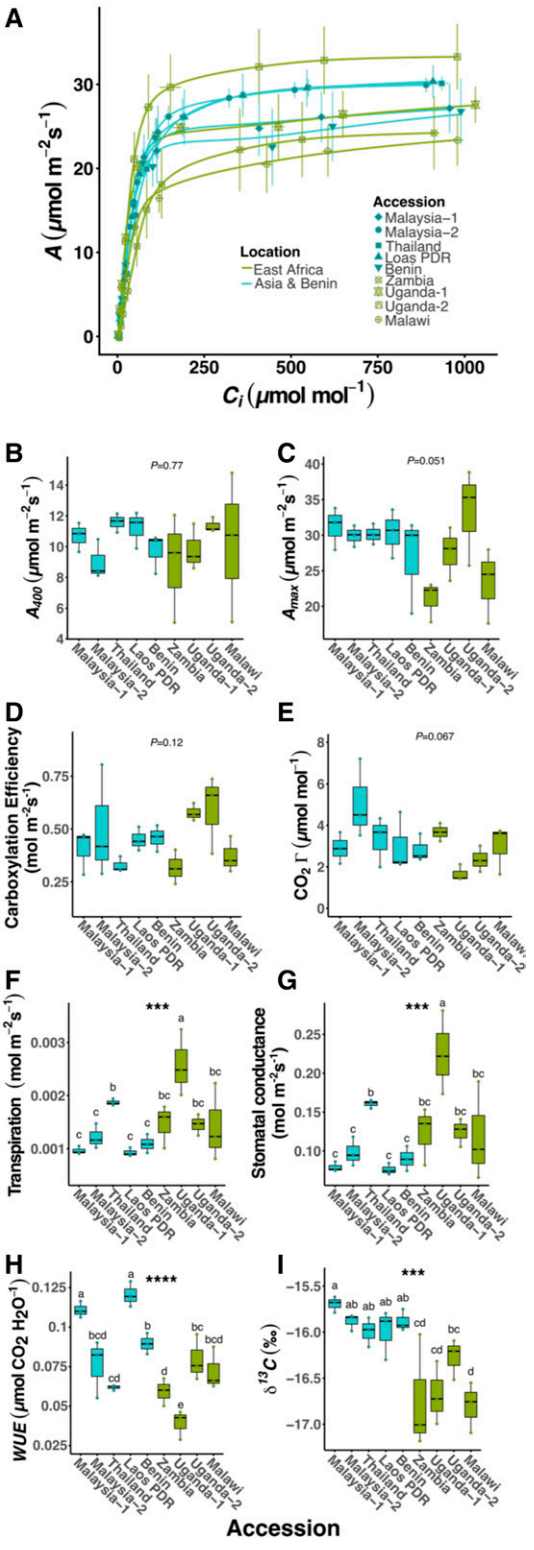

Figure 2. Physiological variation for photosynthetic gas-exchange parameters among a diverse panel of *G. gynandra* accessions. A, *A* versus C_i response curve. B, A_{400} (400 μL L^{-1} atmospheric CO_2 concentration [C_a] and photosynthetic photon flux density [PPFD] of 350 μmol m^{-2} s^{-1}). C, A_{max} (1,200 μL L^{-1} C_a and PPFD of 2,000 μmol m^{-2} s^{-1}). D, Γ. E, Carboxylation efficiency. F, Transpiration. G, Stomatal conductance. H, *WUE*. I, $\delta^{13}C$. Asterisks indicate significant differences between accessions (one-way ANOVA, $n = 3$: ***, $P < 0.001$; and ****, $P < 0.0001$). Letters above individual box-scatterplots indicate significant groupings according to Duncan's multiple range test ($\alpha = 0.05$).

The application of molecular marker-trait associations to study C_4 photosynthesis would expedite the discovery of key regulators to engineer increased photosynthetic efficiency in C_3 plants. However, to our knowledge, there are currently no examples showing that variation in C_4 traits within a single species is sufficient to allow breeding and molecular trait mapping. Interspecific hybrids have been generated between C_3 and C_4 species of the dicotyledon genus *Atriplex* (Oakley et al., 2014). Although the progeny possessed variation in C_4 phenotypes, specific traits showed limited penetrance, and there were high rates of sterility (Brown and Bouton, 1993). In the grass family, *Alloteropsis semialata* shows natural variation in C_4 parameters and has been classified into C_3 or C_4 subspecies (Ueno and Sentoku, 2006; Lundgren et al., 2016), but there are currently no reports that these populations have been bred. Therefore, we investigated the extent to which key C_4 traits varied in the C_4 dicotyledon *Gynandropsis gynandra*, which is a leafy green vegetable (Sogbohossou et al., 2018) in a clade sister to the Brassicaceae that contains both C_3 and C_4 species (Brown et al., 2005; Marshall et al., 2007; Feodorova et al., 2010). Here, we show that accessions of *G. gynandra* show significant variation in both anatomical and physiological traits associated with C_4 photosynthesis. These accessions have short generation spans, are sexually compatible, and produce fertile offspring. Our findings indicate that there is sufficient natural variation to allow the use of classical genetics to identify loci controlling the complex C_4 phenotype.

RESULTS AND DISCUSSION

Accessions of *G. gynandra* were collected from Africa and Asia (Supplemental Table S1). DNA sequencing and phylogenetic reconstruction generated a taxonomy that was consistent with geographical origin but also indicated that the accession from Benin (West Africa) was more similar to Asian accessions than to those from East Africa (Fig. 1A). These accessions displayed considerable variation in macroscopic characteristics associated with leaf appearance (Fig. 1B; Supplemental Fig. S1A). For example, fully expanded leaflets varied in size and shape, and there was variation in petiole length, the presence of trichomes, and anthocyanin pigmentation. As there was considerable macroscopic variation in leaf characteristics, we then evaluated these accessions for variation in features of Kranz anatomy. Interestingly, there were statistically significant differences in vein density (Fig. 1, C and D; Supplemental Fig. S1B), cross-sectional area of BS strands (Fig. 1, C and E; Supplemental Fig. S1C), size of individual BS cells (Fig. 1F), and stomatal density (Fig. 1, C

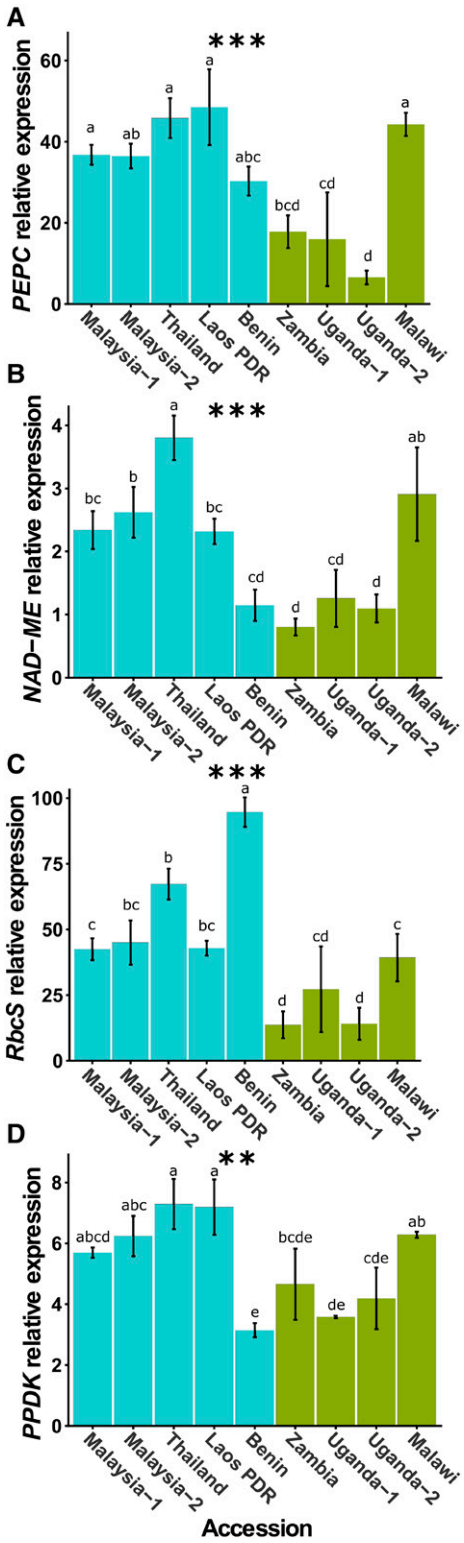

Figure 3. Transcript abundance for key enzymes in the C_4 cycle among diverse *G. gynandra* accessions. Differences in transcript abundance were determined by reverse transcription-quantitative PCR (RT-qPCR) relative to the *ACTIN7* gene. Asterisks indicate significant differences between accessions (one-way ANOVA, $n = 3$: **, $P < 0.01$; and ***, $P < 0.001$). Letters above individual bar charts indicate significant groupings among accessions according to Duncan's multiple range test ($\alpha = 0.05$).

and G). There was no discernible variation in intervein distance or number of BS cells surrounding each vein (Supplemental Fig. S2). However, on average, East African accessions showed higher vein density, reduced distance between veins, and greater stomatal density than Asian accessions (Supplemental Fig. S3, A–C). Asian accessions typically had larger BS areas and cell sizes than those from the African continent (Supplemental Fig. S3, D and E). Vein density was inversely correlated with BS area and BS cell size but positively correlated with stomatal density (Supplemental Table S2). The average number of BS cells around each vein showed no statistically significant differences between lines (Supplemental Fig. S3F), but the cross-sectional area of the BS and the size of individual BS cells were positively correlated ($\rho = 0.8$, $P < 0.0001$). Therefore, we conclude that the area of individual BS cells, rather than the number of these cells per vein bundle, drives the increased BS strand area observed in some accessions. This suggests that genetic determinants of cell size rather than cell proliferation are involved in the variation in BS tissue in *G. gynandra*. Despite the lower phenotypic variation associated with C_4 compared with C_3 leaves (Sage and McKown, 2006), our findings demonstrate that flexibility is still possible within individual species that are fully C_4.

We next investigated whether differences observed in Kranz anatomy affected photosynthetic performance. For all accessions, their CO_2 response curves (assimilation [A] and response to the concentration of CO_2 inside the leaf [C_i]) were typical of C_4 plants, with high carboxylation efficiencies and low CO_2 compensation points (Γ; Fig. 2A; Supplemental Fig. S4A). Parameters associated with instantaneous gas exchange, such as maximum rate of photosynthesis (A_{max}), rate of photosynthesis under the conditions of growth (A_{400}), CO_2 carboxylation efficiencies, and Γ, showed little variation between accessions (Fig. 2, B–E; Supplemental Fig. S4, B–E). As C_4 species typically grow under relatively high light intensities, variation in these traits may become apparent at higher light. In fact, modifications to stomatal density in Arabidopsis impact assimilation rates at high light but not at lower light intensities (Schlüter et al., 2003). Thus, it is possible that, when grown under different conditions, these *G. gynandra* accessions would demonstrate additional variation in photosynthetic characteristics.

There were statistically significant differences in transpiration (Fig. 2F), stomatal conductance (Fig. 2G), and water use efficiency (*WUE*; Fig. 2H). Furthermore, there was also significant variation in the carbon isotope discrimination against ^{13}C ($\delta^{13}C$) in leaf dry matter (Fig. 2I), which is a measure of the efficiency of the C_4 carbon pump over the lifetime of the leaf. Accessions from Asia-Benin showed reduced discrimination against $\delta^{13}C$ compared with the East African lines (Supplemental Fig. S4I). Therefore, these data indicate that accessions of *G. gynandra* possess significant variation in parameters linked to the balance between water use

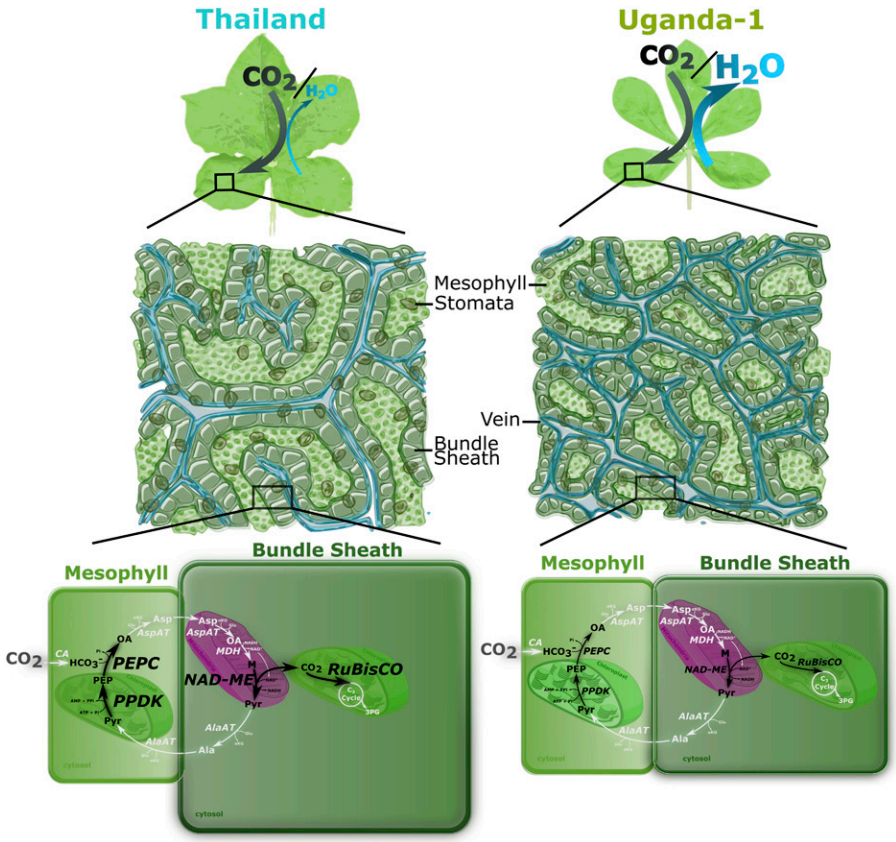

Figure 4. Summary of differences in anatomy, physiology, and C_4-related transcript abundance exhibited by extreme *G. gynandra* accessions. The accessions Thailand and Uganda-1 had larger BS cells, lower vein and stomatal density, and higher *WUE*, $\delta^{13}C$, and transcript abundance of core C_4 cycle enzymes. Differential transcript abundance among accessions is indicated by black arrows, and larger font represents higher relative transcript abundance. Enzymatic steps in white were not investigated.

and photosynthesis that influenced the efficiency of the C_4 cycle over their lifetimes.

We next sought to investigate the extent to which the transcript abundance of core genes in the C_4 cycle differed between the accessions. Interestingly, there were statistically significant differences in the abundance of transcripts encoding phospho*enol*pyruvate carboxylase (*PEPC*), which catalyzes the first committed step of the C_4 cycle, the BS-specific decarboxylase NAD-dependent malic enzyme (*NAD-ME*), the small subunit of Rubisco (*RbcS*), and pyruvate,orthophosphate dikinase (*PPDK*) that regenerates phospho*enol*pyruvate, the primary acceptor of HCO_3^- (Fig. 3). These differences in C_4-related transcript abundance were associated with the geographical location and phylogeny of the accessions, with the accessions from Asia-Benin accumulating greater levels of C_4-related transcripts than those from East Africa (Supplemental Fig. S5, A–D). Understanding how the genes encoding photosynthetic enzymes become strongly expressed and patterned to either M or BS cells of C_4 species is a longstanding area of research. Although progress has been made in identifying the cis-elements responsible for this phenomenon, little is known about the transcription factors involved. Therefore, the intraspecific variation in expression of genes encoding enzymes of the C_4 cycle in *G. gynandra* provides an opportunity to identify trans-factors important for C_4 photosynthesis. Despite accessions functioning with similar photosynthetic efficiencies under ambient CO_2 and light conditions, when assessed by phylogenetic grouping, those with more pronounced Kranz traits (e.g. larger BS tissues and lower vein densities) exhibited increased A_{max}, *WUE*, and $\delta^{13}C$ (Supplemental Fig. S4, C, H, and I) and stronger expression of the core genes of the C_4 cycle (Supplemental Fig. S5). To summarize, there were striking differences between accessions, such that some possessed higher *WUE*, lower density of stomata and veins, larger BS areas and cell sizes, higher $\delta^{13}C$ (indicative of a stronger C_4 cycle), and increased expression of genes encoding C_4 enzymes (Fig. 4).

The considerable variation reported in this study offers a valuable germplasm resource to identify regulators of the C_4 pathway and Kranz anatomy through genetic mapping. All accessions in this study

hybridize easily. Emasculation and pollination need only take 15 to 30 s per flower. For example, the most divergent accessions regarding anatomy, Malaysia-1 × Malawi, Malaysia-2 × Malawi, and their reciprocal crosses, produce an average 52 ± 11 seeds per silique (n = 6), whose offspring are fully fertile. The F1 hybrids displayed intermediate characteristics, differing in leaflet number, presence of trichomes on the petiole, and leaf size and shape (Supplemental Fig. S6). Therefore, these hybrid populations provide a breeding foundation to delineate regulatory mechanisms. More broadly, the discovery of intraspecific variation in a C_4 grass would be particularly useful in mapping traits relevant to improving photosynthesis in crops and, thus, introduce C_4 photosynthesis into C_3 cereals.

While our understanding of the regulatory mechanisms underlying C_4 metabolism is growing, there is still a significant gap in tools to expand our understanding of the regulation behind Kranz anatomy and the C_4 biochemical cycle. Methods such as quantitative trait locus mapping or genome-wide association studies in *G. gynandra* or an equally diverse C_4 species may provide insights into the regulation of Kranz development. In this study, most trait variation in *G. gynandra* was associated with characteristics relating to water use that impact carbon capture. It is noteworthy that modifications to C_3 leaves considered to represent early steps on the path toward the C_4 phenotype also are associated with water use rather than CO_2 fixation (Sage, 2004; Williams et al., 2013). As natural vegetation is not considered to be under strong selection pressure to optimize photosynthesis (Long et al., 2015; Ort et al., 2015), it seems likely that C_4 trait variation continues to be driven at least partially through the optimization of water use rather than photosynthesis per se.

MATERIALS AND METHODS

Plant Accessions and Growth Conditions

A selection of nine diverse accessions of *Gynandropsis gynandra* was made from a larger germplasm collection based on initial phenotypic and genetic screening. Five accessions were from Africa and four from Asia (Supplemental Table S1; materials available on request from M.E.S.). Plants from all *G. gynandra* accessions were grown under identical conditions prior to sampling. After germination, all seeds were planted in 5:1 F2 compost (Levington Advance):fine vermiculite premixed with 0.17 g L^{-1} insecticide (Imidasect 5GR; Fargro) in 5-cm^3 cells. Seedlings were kept in a growth chamber at 350 µmol photons m^{-2} s^{-1} PPFD, with a 16-h photoperiod, at 25°C, 60% relative humidity (RH), and ambient [CO_2]. A single dose of 3 mL L^{-1} slow-release 17N-9P-11K fertilizer (All Purpose Continuous Release Plant Food; Miracle-Gro) was applied after 1.5 weeks. Plants for physiological measurements were grown under identical conditions to those for Kranz measurements for the first 3 weeks, after which the plants for Kranz measurements were assayed and the plants for physiological measurements were replanted in 13-cm^3 pots with a 5:1 M3 soil (Levington Advance):medium vermiculite soil mixture and moved to a growth room set to 23°C, 60% RH, ambient [CO_2], and 350 µmol photons m^{-2} s^{-1} PPFD with a 16-h photoperiod. All plants were watered by an automated system whereby the bottom of the trays containing the 13-cm^3 pots was flooded to a depth of 4 cm every 48 h for 10 min, following which the irrigation water was drained.

DNA Sequencing and Phylogenetic Analyses

Genomic DNA was extracted using a cetyltrimethylammonium bromide extraction method. Briefly, leaf samples were ground uniformly in 300 µL of cetyltrimethylammonium bromide extraction buffer containing 2% (w/v) polyvinylpyrrolidone-40 and 1.7% (v/v) β-mercaptoethanol. After vortexing, samples were incubated at 65°C for 30 min, and 300 µL of 24:1 chloroform:isoamyl alcohol was then added. After vortexing and centrifugation, 300 µL of supernatant was removed and placed in 300 µL of isopropanol. DNA was precipitated overnight at −20°C and then centrifuged at full speed for 15 min. The supernatant was removed, the pellet was washed with 200 µL of 96% (v/v) ethanol prior to drying, and the DNA was resuspended in nuclease-free water.

To generate a phylogeny for the accessions, internal transcribed spacer (ITS) regions were sequenced using universal primers ITS 1 and ITS 4, following a protocol published previously (White et al., 1990). In short, ITS regions I and II and the 5.8 S polycistronic rRNA precursor transcribed region were amplified by PCR. These PCR products were purified, and fragments were sequenced. Sequences were then aligned using the MAFFT online server (MAFFT version 7; https://mafft.cbrc.jp/alignment/server/), and a best scoring maximum likelihood tree was generated with RAxML version 8.0.0 on the CIPRES science gateway (Miller et al., 2010).

Preparation of Leaf Tissue Sections for Kranz Measurements

Three weeks after germination, tissue was harvested from healthy plants from the center trifoliate leaves of the second pair of fully expanded true leaves. A 3-mm^2 rectangle was cut from the leaf adjacent to the midvein with a razor blade for transverse sections. Two slightly larger rectangles were cut from identical regions for paradermal sectioning and RT-qPCR analysis.

For transverse sections, leaf tissue in plastic cuvettes was submerged in a 4% (v/v) paraformaldehyde in PBS solution (Sigma-Aldrich), placed in a vacuum chamber for 1 h, and incubated at 4°C overnight for fixing. Cuvettes then underwent an ethanol dehydration series from 30% to 90% (v/v) ethanol solutions (Thermo Fisher Scientific) in 10% (v/v) increments for 45 min each at 4°C with a final overnight treatment at 4°C in 95% ethanol with 0.1% (w/v) eosin dye solution (Sigma-Aldrich). The dye solution was washed three times with 100% (v/v) ethanol at room temperature. The samples were embedded in resin according to the Technovit 7100 (Kulzer) manufacturer's protocol. Hardened resin blocks were cut with a manual rotary microtome (Thermo Fisher Scientific). Sections were placed on microscope slides and stained with 0.1% (w/v) Toluidine Blue solution (Sigma-Aldrich) prior to imaging on a light microscope.

For paradermal sections, fresh tissue samples were placed in plastic cuvettes and incubated in 3:1 100% (v/v) ethanol:acetic acid solution before treatment with 70% (v/v) ethanol solution (refreshed once) at 37°C overnight. To clear the samples, cuvettes were submerged in 5% NaOH solution for 3 h at 37°C, rinsed twice with 70% (v/v) ethanol, and stored at 4°C. After storage, the samples were stained with a 0.1% (v/v) eosin dye in 95% (v/v) ethanol solution. Samples were stored overnight at 4°C and washed with 70% (v/v) ethanol three times before transfer to slides for imaging. To determine stomatal density, impressions of the abaxial epidermis of each central leaflet were generated by applying a thin coat of transparent nail varnish (Boots). After drying, the varnish was peeled off and mounted onto a glass slide for imaging.

Measurement of Kranz Anatomy Traits

Slides of all leaf sections were imaged with an Olympus BX41 light microscope with a mounted Micropublisher 3.3 RTV camera (Q Imaging). Images were captured with Q-Capture Pro 7 software, and measurements were analyzed with the software ImageJ (Schneider et al., 2012). To maximize comparability, strict criteria were applied for all image analyses. Microscopy of transverse leaf sections was used to quantify the BS in terms of average BS tissue area (the total cross-sectional area of all BS cells immediately surrounding a vein) and BS cell size (the average cross-sectional area of individual BS cells around the vein). To quantify BS tissue area, the freehand selection tool was used to subtract the integrated area of each vein from the integrated area of all BS cells in direct contact with the vein on images with 200× total magnification. This value was divided by the number of BS cells in each vein bundle to

obtain the average BS cell size. For intervein distance (the distance between the centers of adjacent veins in transverse sections), only vein bundles were measured for which the following criteria did not apply: wide (indicates branching) or extremely large veins, veins with distorted BS cells due to contact with adjacent BS tissues (indicates merging), and veins with damaged BS cells. The line selection tool was used to measure the linear distance between the centers of adjacent veins on images with 40× total magnification. Vein density (vein length per unit area of leaf) was quantified on paradermal sections on images with 100× total magnification. Slides were imaged with the same microscopy equipment as transverse sections but set to Ph3 (phase contrast). Three images (from three different leaves per plant) were randomly selected for measurement. The freehand line tool was used to trace all veins (both major and minor) along their center. As it was not possible to trace all veins in an image simultaneously, individual vein sections were measured progressively without overlap and the individual lengths summed. The total vein length was divided by the image area to obtain the density. Stomatal density (the number of stomata per unit area of leaf) was measured on three subsampled leaves from three random plants on images with 200× total magnification. The total number of stomata was divided by the image area to obtain the density.

Photosynthetic Performance

An LI-6800 portable photosynthesis infrared gas analyzer system (LI-COR) equipped with a multiphase flash fluorimeter was used to assess physiological differences for photosynthetic parameters between *G. gynandra* accessions. All physiological measurements were performed on the central leaflet of three independent 5-week-old plants, grown in separate pots. For stomatal conductance, transpiration (E), and A_{400}, measurements were taken during ambient conditions of growth (400 µL L^{-1} C_a and PPFD of 350 µmol m^{-2} s^{-1}). *WUE* was defined as A_{400}/E. A combination chlorophyll fluorescence and A/C_i curve was measured for three plants from each accession. C_a reference values were 400, 400, 300, 200, 100, 50, 25, 400, 400, 400, 600, 800, 1,000, 1,200, and 400 µL L^{-1}, with a saturating rectangular pulse of 12,000 µmol m^{-2} s^{-1} at each reference point. Otherwise, measurements were made at a PPFD of 2,000 µmol m^{-2} s^{-1}, 23°C, and 60% RH at each reference point. All leaves covered the full area of the cuvette. Measurements were carried out on consecutive days between 1 and 8 h postdawn, measuring one plant selected at random from each accession per day. Rates of gas exchange including A_{max} at 1,200 µL L^{-1} C_a represent the measurements made, but a line of best fit also was plotted to fit the A/C_i response data to a logarithmic trend using the generalized additive model feature of the tidyverse package in R. Γ was calculated using linear regression of A and C_i measurements made between C_a of 25 to 200 µL L^{-1} (Sharkey, 1988). Adjusted R^2 values for all regression lines ranged between 0.993 and 0.997. Carboxylation efficiency was calculated as the partial derivative $\frac{\partial A}{\partial C_i}$ *at* $A = 0$. $\delta^{13}C$ analysis was performed according to methods described previously (Royles et al., 2016) on three biological replicates per accession with 500 µg of dried leaf tissue.

Statistical Analysis

For all tests, individual plants were considered experimental units in a complete randomized design. Data were analyzed in SAS (University Version; SAS Institute) and in R (version 3.4.2; R Studio). The R packages agricolae, car, cowplot, dplyr, ggplot2, multcompView, and tidyverse were used for data analysis and downloaded via the Install Packages Tool in RStudio (version 1.0.143; R Studio). A one-way ANOVA ($\alpha = 0.05$) with type III sums of squares, which accounts for unequal replication, compared all means from anatomical and physiological measurements among *G. gynandra* accessions, and Student's t test ($\alpha = 0.05$) was used to compare means of accessions by phylogenetic proximity, using the PROC GLM and PROC TTEST functions in SAS, respectively. Null hypotheses were rejected for specific ANOVAs or Student's t tests for any population with $P \leq 0.05$. Levene's test was used to evaluate homoscedasticity and was centered at the median (Levene, 1960) using the car package in R. All analyses showed equal variance ($\alpha = 0.05$), except for the number of BS cells (Supplemental Table S3). Duncan's multiple range posthoc test was used for mean separation on accessions ($\alpha = 0.05$) with statistically significant ANOVAs in the R package agricolae (Duncan, 1955). To provide conservative lower type I experiment error rates, Tukey's studentized range test (HSD) also was used ($\alpha = 0.05$) with statistically significant ANOVAs in SAS and was plotted in R with the packages dplyr and multcompView (Supplemental Fig. S7). Pearson product-moment correlation coefficients were calculated to find associations among features of Kranz traits (Pearson, 1895) using the PROC CORR function in SAS. Linear regression was performed using the PROC REG function in SAS to calculate Γ and carboxylation efficiency. The total number of replicates used in each experiment is summarized in Supplemental Table S4.

Analysis of Transcript Abundance

Leaf tissue samples for RNA extraction were harvested simultaneously with samples for Kranz trait measurements after 3 weeks of growth using the opposite paired trifoliate leaf to that harvested for sectioning and imaging. These fresh leaf samples were immediately flash frozen with liquid nitrogen and stored at −80°C. Total RNA was extracted from three tissue samples per accession with an RNeasy Mini Kit (Qiagen) according to the manufacturer's instructions. An on-column DNase digestion protocol was applied to remove genomic DNA contamination (Qiagen) before cDNA was synthesized with Invitrogen SuperScript II reverse transcriptase enzyme according to the manufacturer's instructions (Thermo Fisher Scientific). All cDNA samples were stored at −20°C before RT-qPCR. Primers were designed for quantitative PCR of the C_4 cycle genes *PEPC*, *NAD-ME*, *RbcS*, and *PPDK* (Supplemental Table S5), and reactions were carried out as reported previously (Burgess et al., 2016) on three biological and three technical replicates.

Accession Numbers

Sequence data from this article can be found in the GenBank/EMBL data libraries under accession numbers MH188307 to MH188315.

Supplemental Data

The following supplemental materials are available.

Supplemental Figure S1. Representative images for macroscopic and microscopic variation in leaf anatomy across a panel of *G. gynandra* accessions.

Supplemental Figure S2. Nonvariable features of Kranz anatomy among accessions.

Supplemental Figure S3. Natural variation in features of Kranz anatomy between *G. gynandra* accessions from Asia-Benin and those from East Africa.

Supplemental Figure S4. Physiological variation for photosynthetic gas-exchange parameters between *G. gynandra* accessions from Asia-Benin and those from East Africa.

Supplemental Figure S5. Transcript abundance differences for key enzymes in the C_4 cycle between *G. gynandra* phylogenetic clusters.

Supplemental Figure S6. Leaf appearance of F1 hybrids between *G. gynandra* lines that exhibited the greatest differences in Kranz features.

Supplemental Figure S7. Quantitative natural variation among diverse *G. gynandra* accessions controlling for lower type I error rates.

Supplemental Table S1. Accessions of *G. gynandra* investigated and their source regions.

Supplemental Table S2. Pearson product-moment correlation coefficients for Kranz anatomy traits.

Supplemental Table S3. Summary statistics for Levene's test for homogeneity of variance for individual ANOVAs ($\alpha = 0.05$).

Supplemental Table S4. The number of replicates for anatomical measurements.

Supplemental Table S5. List of primers for RT-qPCR analyses.

ACKNOWLEDGMENTS

We thank Frank Becker and Beatrice Landoni (Wageningen University) for providing ITS sequence data and initial information on the selected lines, Blandine Gilbert for help with image processing, and James Rolfe for carbon isotope analysis.

Received February 9, 2018; accepted March 30, 2018; published April 20, 2018.

LITERATURE CITED

Akyildiz M, Gowik U, Engelmann S, Koczor M, Streubel M, Westhoff P (2007) Evolution and function of a cis-regulatory module for mesophyll-specific gene expression in the C4 dicot *Flaveria trinervia*. Plant Cell **19**: 3391–3402

Aubry S, Kelly S, Kümpers BMC, Smith-Unna RD, Hibberd JM (2014) Deep evolutionary comparison of gene expression identifies parallel recruitment of *trans*-factors in two independent origins of C4 photosynthesis. PLoS Genet **10**: e1004365

Bowes G, Ogren WL, Hageman RH (1971) Phosphoglycolate production catalyzed by ribulose diphosphate carboxylase. Biochem Biophys Res Commun **45**: 716–722

Bräutigam A, Gowik U (2016) Photorespiration connects C3 and C4 photosynthesis. J Exp Bot **67**: 2953–2962

Bräutigam A, Schliesky S, Külahoglu C, Osborne CP, Weber APM (2014) Towards an integrative model of C4 photosynthetic subtypes: insights from comparative transcriptome analysis of NAD-ME, NADP-ME, and PEP-CK C4 species. J Exp Bot **65**: 3579–3593

Brown HR, Bouton JH (1993) Physiology and genetics of interspecific hybrids between photosynthetic types. Annu Rev Plant Physiol Plant Mol Biol **44**: 435–456

Brown NJ, Newell CA, Stanley S, Chen JE, Perrin AJ, Kajala K, Hibberd JM (2011) Independent and parallel recruitment of preexisting mechanisms underlying C4 photosynthesis. Science **331**: 1436–1439

Brown NJ, Palmer BG, Stanley S, Hajaji H, Janacek SH, Astley HM, Parsley K, Kajala K, Quick WP, Trenkamp S, (2010) C4 acid decarboxylases required for C4 photosynthesis are active in the mid-vein of the C3 species Arabidopsis thaliana, and are important in sugar and amino acid metabolism. Plant J **61**: 122–133

Brown NJ, Parsley K, Hibberd JM (2005) The future of C4 research: maize, Flaveria or Cleome? Trends Plant Sci **10**: 215–221

Burgess SJ, Granero-Moya I, Grangé-Guermente MJ, Boursnell C, Terry MJ, Hibberd JM (2016) Ancestral light and chloroplast regulation form the foundations for C4 gene expression. Nat Plants **2**: 16161

Duncan DB (1955) Multiple range and multiple F tests. Biometrics **11**: 1–42

Eastmond PJ, Astley HM, Parsley K, Aubry S, Williams BP, Menard GN, Craddock CP, Nunes-Nesi A, Fernie AR, Hibberd JM (2015) Arabidopsis uses two gluconeogenic gateways for organic acids to fuel seedling establishment. Nat Commun **6**: 6659

Feodorova TA, Voznesenskaya EV, Edwards GE, Roalson EH (2010) Biogeographic patterns of diversification and the origins of C4 in Cleome (Cleomaceae). Syst Bot **35**: 811–826

Garner DMG, Mure CM, Yerramsetty P, Berry JO (2001) Kranz anatomy and the C4 pathway. eLS

Heckmann D, Schulze S, Denton A, Gowik U, Westhoff P, Weber APM, Lercher MJ (2013) Predicting C4 photosynthesis evolution: modular, individually adaptive steps on a Mount Fuji fitness landscape. Cell **153**: 1579–1588

Hibberd JM, Covshoff S (2010) The regulation of gene expression required for C4 photosynthesis. Annu Rev Plant Biol **61**: 181–207

Hibberd JM, Quick WP (2002) Characteristics of C4 photosynthesis in stems and petioles of C3 flowering plants. Nature **415**: 451–454

Kajala K, Brown NJ, Williams BP, Borrill P, Taylor LE, Hibberd JM (2012) Multiple Arabidopsis genes primed for recruitment into C4 photosynthesis. Plant J **69**: 47–56

Langdale JA (2011) C4 cycles: past, present, and future research on C4 photosynthesis. Plant Cell **23**: 3879–3892

Lauterbach M, Schmidt H, Billakurthi K, Hankeln T, Westhoff P, Gowik U, Kadereit G (2017) *De novo* transcriptome assembly and comparison of C3, C3-C4, and C4 species of tribe Salsoleae (Chenopodiaceae). Front Plant Sci **8**: 1939

Levene H (1960) Robust tests for equality of variances. *In* **O Ingram, H Harold**, eds, Contributions to Probability and Statistics: Essays in Honor of Harold Hotelling. Stanford University Press, Stanford, CA, pp 278–292

Long SP, Marshall-Colon A, Zhu XG (2015) Meeting the global food demand of the future by engineering crop photosynthesis and yield potential. Cell **161**: 56–66

Lundgren MR, Christin PA, Escobar EG, Ripley BS, Besnard G, Long CM, Hattersley PW, Ellis RP, Leegood RC, Osborne CP (2016) Evolutionary implications of C3-C4 intermediates in the grass *Alloteropsis semialata*. Plant Cell Environ **39**: 1874–1885

Lundgren MR, Osborne CP, Christin PA (2014) Deconstructing Kranz anatomy to understand C4 evolution. J Exp Bot **65**: 3357–3369

Mallmann J, Heckmann D, Bräutigam A, Lercher MJ, Weber APM (2014) The role of photorespiration during the evolution of C4 photosynthesis in the genus Flaveria. eLife **3**: e02478

Marshall DM, Muhaidat R, Brown NJ, Liu Z, Stanley S, Griffiths H, Sage RF, Hibberd JM (2007) *Cleome*, a genus closely related to *Arabidopsis*, contains species spanning a developmental progression from C3 to C4 photosynthesis. Plant J **51**: 886–896

Mauricio R (2001) Mapping quantitative trait loci in plants: uses and caveats for evolutionary biology. Nat Rev Genet **2**: 370–381

Miller M, Pfeiffer W, Schwartz T (2010) Creating the CIPRES Science Gateway for inference of large phylogenetic trees. *In* 2010 Gateway Computing Environments Workshop. GCE, pp 1–8

Oakley JC, Sultmanis S, Stinson CR, Sage TL, Sage RF (2014) Comparative studies of C3 and C4 Atriplex hybrids in the genomics era: physiological assessments. J Exp Bot **65**: 3637–3647

Ort DR, Merchant SS, Alric J, Barkan A, Blankenship RE, Bock R, Croce R, Hanson MR, Hibberd JM, Long SP, (2015) Redesigning photosynthesis to sustainably meet global food and bioenergy demand. Proc Natl Acad Sci USA **112**: 8529–8536

Pearson K (1895) Notes on regression and inheritance in the case of two parents. Proc R Soc Lond **58**: 240–242

Reeves G, Grangé-Guermente MJ, Hibberd JM (2017) Regulatory gateways for cell-specific gene expression in C4 leaves with Kranz anatomy. J Exp Bot **68**: 107–116

Reyna-Llorens I, Burgess SJ, Reeves G, Singh P, Stevenson SR, Williams BP, Stanley S, Hibberd JM (2018) Ancient duons may underpin spatial patterning of gene expression in C4 leaves. Proc Natl Acad Sci USA **115**: 1931–1936

Royles J, Amesbury MJ, Roland TP, Jones GD, Convey P, Griffiths H, Hodgson DA, Charman DJ (2016) Moss stable isotopes (carbon-13, oxygen-18) and testate amoebae reflect environmental inputs and microclimate along a latitudinal gradient on the Antarctic Peninsula. Oecologia **181**: 931–945

Sage RF (2004) Tansley review. The evolution of C4 photosynthesis. New Phytol **161**: 30

Sage RF (2016) A portrait of the C4 photosynthetic family on the 50th anniversary of its discovery: species number, evolutionary lineages, and Hall of Fame. J Exp Bot **67**: 4039–4056

Sage RF, McKown AD (2006) Is C4 photosynthesis less phenotypically plastic than C3 photosynthesis? J Exp Bot **57**: 303–317

Schlüter U, Muschak M, Berger D, Altmann T (2003) Photosynthetic performance of an Arabidopsis mutant with elevated stomatal density (*sdd1-1*) under different light regimes. J Exp Bot **54**: 867–874

Schneider CA, Rasband WS, Eliceiri KW (2012) NIH Image to ImageJ: 25 years of image analysis. Nat Methods **9**: 671–675

Sharkey TD (1988) Estimating the rate of photorespiration in leaves. Physiol Plant **73**: 147–152

Sogbohossou EOD, Achigan-Dako EG, Maundu P, Solberg S, Deguenon EMS, Mumm RH, Hale I, Van Deynze A, Schranz ME (2018) A roadmap for breeding orphan leafy vegetable species: a case study of *Gynandropsis gynandra* (Cleomaceae). Hortic Res **5**: 2

Ueno O, Sentoku N (2006) Comparison of leaf structure and photosynthetic characteristics of C3 and C4 *Alloteropsis semialata* subspecies. Plant Cell Environ **29**: 257–268

White T, Bruns T, Lee S, Taylor J (1990) Amplification and direct sequencing of fungal ribosomal RNA genes for phylogenetics. PCR Protoc **18**: 315–322

Williams BP, Burgess SJ, Reyna-Llorens I, Knerova J, Aubry S, Stanley S, Hibberd JM (2016) An untranslated cis-element regulates the accumulation of multiple C4 enzymes in *Gynandropsis gynandra* mesophyll cells. Plant Cell **28**: 454–465

Williams BP, Johnston IG, Covshoff S, Hibberd JM (2013) Phenotypic landscape inference reveals multiple evolutionary paths to C4 photosynthesis. eLife **2**: e00961